PAPER

Percolation and jamming properties in an object growth model on a triangular lattice with finite-size impurities

View the article online for updates and enhancements.

Percolation and jamming properties in an object growth model on a triangular lattice with finite-size impurities

D Dujak[1,*], A Karač[2], Lj Budinski-Petković[3], Z M Jakšić[4] and S B Vrhovac[4]

[1] Faculty of Electrical Engineering, University of Sarajevo, Sarajevo 71000, Bosnia and Herzegovina
[2] Polytechnic Faculty, University of Zenica, Zenica, Bosnia and Herzegovina
[3] Faculty of Engineering, University of Novi Sad, Trg D. Obradovića 6, Novi Sad 21000, Serbia
[4] Institute of Physics Belgrade, University of Belgrade, Pregrevica 118, Zemun 11080, Belgrade, Serbia
E-mail: ddujak@etf.unsa.ba

Abstract. A percolation model with nucleation and object growth is studied by Monte Carlo simulations on a triangular lattice with finite-size impurities. The growing objects are needle-like objects and self-avoiding random walk chains. Results are obtained for three different shapes of impurities covering three lattice sites—needle-like, angled and triangular. In each run through the system, the lattice is initially randomly occupied by impurities of a specified shape at a given concentration ρ_{imp}. Then, the seeds for the object growth are randomly distributed at a given concentration ρ. The percolation and jamming properties of the growing objects are compared for the three different impurity shapes. For all the impurity shapes, the percolation thresholds θ_p^* have lower values in the growing needle-like objects than in the growing self-avoiding random walk chains. In the presence of needle-like and angled impurities, the percolation threshold increases with the impurity concentration for a fixed seed density. The percolation thresholds have the highest values in the needle-like impurities, and

---

* Author to whom any correspondence should be addressed.

somewhat lower values in the angled impurities. On the other hand, in the presence of the triangular impurities, the percolation threshold decreases with the concentration of impurities.

Keywords: percolation, triangular lattice, seeded growth, impurities

Contents

1. Introduction

Nanoparticles and other low-dimensional nanostructures are the subject of great scientific interest, significantly influencing technologically important and health-relevant areas. Nanotechnology has contributed to nanocatalysis [1–3], electronics [4], photonics [5], information storage [6], imaging [7] and various biomedical applications [8–10]. The properties of nanoparticles are related to their size and shape. One can fine-tune nanoparticles' photochemical, catalytic, magnetic and electronic properties by controlling these structural characteristics. In fact, there are many factors that influence the outcome of the nanoparticle growth process, such as size [11], temperature [12], chemical environment and addition of surfactants/capping agents [13]. Seeded growth has emerged as a compelling method to create a wide variety of nanocrystal samples [14–18]. Random sequential adsorption (RSA) on a lattice is often used as a basic model for describing particle growth by aggregation [19].

RSA is a process in which particles of different shapes and sizes are constantly trying to attach themselves to a random location on a surface. If the incoming particle does not overlap any previously attached particles, then it binds irreversibly. A quantity of central interest is the fraction of the total area covered by the depositing particles

$\theta(t)$. Because of the blocking effect by the already deposited particles of the substrate available for deposition of additional particles, the limiting value θ_J is less than the close packing [20–22]. The formation of the limiting jammed state is governed by the infinite memory correlation effects, due to the absence of relaxation.

During the process of RSA, the number of deposited objects on the substrate increases so that they form clusters. A cluster is a group of occupied sites in such a way that each site has at least one occupied nearest-neighbor site. Percolation assumes the existence of a large cluster that extends from one side to the opposite side of the system. Basically, percolation theory is based on finding the minimum coverage fraction for which a complete path of adjacent sites crossing the entire system becomes possible. This value of the fraction of the total area is called the effective percolation threshold $\theta_{\rm p}$. The formation of long-range connectivity in disordered systems attracts considerable interest due to its applications in numerous practical problems, such as conductivity in composite materials, flow through porous media, polymerization, gelation and the behavior of scale-free random networks [23–29].

Recently, we proposed an artificial but instructive model, which is able to reproduce the granular growth, from nucleation to percolation, and for different growing shapes on a triangular lattice [30, 31]. This model can be regarded as a very simple picture of the size- and shape-controlled nanoparticles' growth. In fact, we numerically examined a percolation model with nucleation and simultaneous growth of multiple finite clusters, taking the initial seed concentration ρ as a tunable parameter [18, 32, 33]. As growing objects of predefined shape, we considered needle-like objects, random walk chains and 'wrapping' objects, whose size is gradually increased by wrapping the walks in several different ways, making triangles, rhombuses and hexagons. For the growing needle-like objects and the growing random walk chains, the percolation threshold θ_p^* increases with the seed density ρ for lower values of ρ, reaches a broad maximum and slightly falls for higher values of the seed density. The growing random walk chains cover the surface more efficiently than the needle-like objects, and percolation is reached at higher coverages in the growing random walk chains. The percolation threshold is most affected by the way the object grows at low seed concentrations.

When modeling real deposition processes, one often has to consider some contaminations (impurities) that disturb the deposition of primary particles and introduce disorder into the system. The surfaces may be chemically heterogeneous and contain defects [34], or may be prepatterned [35]. Cornette *et al* [36, 37] numerically investigated both the bond and the site percolation problems for linear k-mers and self-avoiding walks in the presence of impurities. The contaminated lattice was built by randomly selecting a fraction of bonds or sites that were considered forbidden for deposition. This research suggested that the concentration of impurities at which percolation becomes impossible decreases rapidly with increasing values of k. Centers and Ramirez-Pastor [38] investigated a similar system and reported that for each fixed value of k, percolation can occur when a fraction of imperfect bonds is smaller than the critical concentration of defects.

Tarashevich *et al* [39, 40] studied the influence of defects on the behavior of electrical conductivity in a monolayer produced by the isotropic and anisotropic deposition of k-mers onto a square lattice. Two kinds of defects were taken into consideration. In the first one, it was assumed that nonconducting point defects initially occupied some

fractions of the sites, and in the second one, some fractions of the sites in the k-mers were nonconducting. Calculation of the electrical conductivities explicitly confirmed that even a very small concentration of defects has a strong impact on the electrical conductivity. Above some critical concentrations of defects, percolation was found to be blocked, even at the jamming limit.

The percolation properties of the deposition process on a triangular lattice with extended impurities were studied in [41]. For needle-like impurities of various lengths ℓ at various concentrations p, the percolation threshold θ_{p}^* was determined for k-mers, angled objects and triangles of two different sizes. For sufficiently large impurities, the percolation threshold θ_{p}^* of all examined objects was found to increase with the concentration p, and this increase was more prominent for impurities of larger length ℓ.

Irreversible deposition of two types of objects, linear k-mers and self-avoiding random walks (SARWs), covering k lattice sites was simulated on a square lattice with randomly distributed impurities [42]. The lattice was considered 'contaminated' with impurities in a fraction c $(0 \leqslant c < 1)$. For all examined objects, linear k-mers and SARWs, the jamming coverage θ_J decreases as the concentration of impurities increases for a fixed object length. Also, θ_J is found to be a monotonic decreasing function of k for a fixed value of c. SARWs, for a given k and c, give higher jamming coverages than the linear k-mers.

Here, we present the results of Monte Carlo simulations of the seed growth on surfaces with impurities of various shapes on a triangular lattice. We consider three different shapes of impurities covering three lattice sites—needle-like, angled and triangular. We compare the results of the percolation thresholds and jamming coverages for growing needle-like objects and growing random walk chains. The aim of this work is to investigate how seed growth and the deposit formation are affected by the shape of defects present in the lattice.
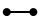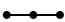
The paper is organized as follows. Section 2 describes the details of the model and the simulations. The results and discussions are given in section 3, while section 4 contains some additional comments and final remarks.

2. Definition of the model

The substrate for the object growth is a two-dimensional (2D) triangular lattice of size L with finite-size impurities of various shapes. Namely, there is a finite number of different shapes that can be made by SARWs of length ℓ, and such shapes are given in table 1 for $\ell = 1$ and $\ell = 2$. The impurities are of needle-like, angled and triangular shapes, covering three lattice sites—objects (B), (C) and (D) in table 1. In each run through the system, the lattice is initially randomly occupied by needle-like, angled or triangular impurities at a given concentration ρ_{imp}, and by the monomer seeds for the object growth randomly distributed at a given concentration ρ. Both of these distributions are obtained via the RSA process. The concentrations ρ_{imp} and ρ are defined as fractions of the lattice sites occupied by impurities and seeds, respectively.

After the initial configuration is prepared, a random growing process is initiated in the system. Two kinds of growing objects are considered: needle-like shapes (k-mers) of length $\ell = k - 1$, and the shapes made by SARW chains.

Table 1. Various shapes made by self-avoiding walks of length $\ell = 1$ and $\ell = 2$. The number of nearest neighbors is denoted by $m^{(x)}$ for the corresponding shape, and ℓ denotes the length of the walk that makes the shape.

(x)	Shape	$m^{(x)}$	$\ell^{(x)}$
(A)	•—•	8	1
(B)	•—•—•	10	
(C)	╱	10	2
(D)	⋀	9	

At each Monte Carlo step, a lattice site occupied by a seed is selected at random. Then, an unoccupied adjacent site is selected at random according to the rules for the object growth—the needle-like objects or the SARW chains, as shown in figure 1. In the needle-like shapes, the chosen k-mer extends in the direction of the first step in the formation of the depositing object. For illustration, the possible growth directions of individual seeds are shown by red dashed lines in figure 1(a). If the corresponding adjacent site is occupied by an impurity or by the previously deposited object, the attempted k-mer growth is not possible and the object remains unchanged. In random walk chains, the selected chain randomly extends into one of the empty nearest-neighbor sites. Examples of the growth of some random chains are illustrated in figure 1(b), where the red dashed lines represent the possible directions of the growth in the next Monte Carlo step. If all nearest-neighbor sites are occupied, the chosen chain does not change.

Growth of the objects leads to the contact of two objects when they are separated by a single lattice spacing. Then, they are merged into a single cluster. During the growth of these clusters, two clusters may come into contact. Two clusters separated by a single lattice spacing are amalgamated into a single cluster. The coverage of the surface is increased in the process up to the percolation threshold θ_{p}, when a cluster that extends through the whole system appears. Conventional boundary conditions (percolation on a torus) have been used throughout the paper without loss of generality, i.e. sites on an open border are connected to corresponding sites on the opposite border. A tree-based union and find algorithm was used to determine the percolation threshold [43]. Each cluster of connected sites is stored as a separate tree, with a single 'root' site. All the sites in the cluster possess pointers to the root site; therefore, it is simple to ascertain whether two sites are members of the same cluster. When two separate clusters connect, they are amalgamated by adding a pointer from the root of the smaller cluster to the root of the larger one.

During the simulation, each growing object is examined for possible growth. The jamming limit θ_J is reached when no object can grow anymore. Objects that have no empty sites for further growth are removed from the list of dialing objects. The simulation stops when there are no more objects in the list. Data are averaged over 500 independent runs through the system for each lattice dimension and for each set of parameters.

It is well-established that correlations in RSA decay extremely fast [19, 44, 45]. As a result, high-precision results can be obtained numerically on relatively small lattices
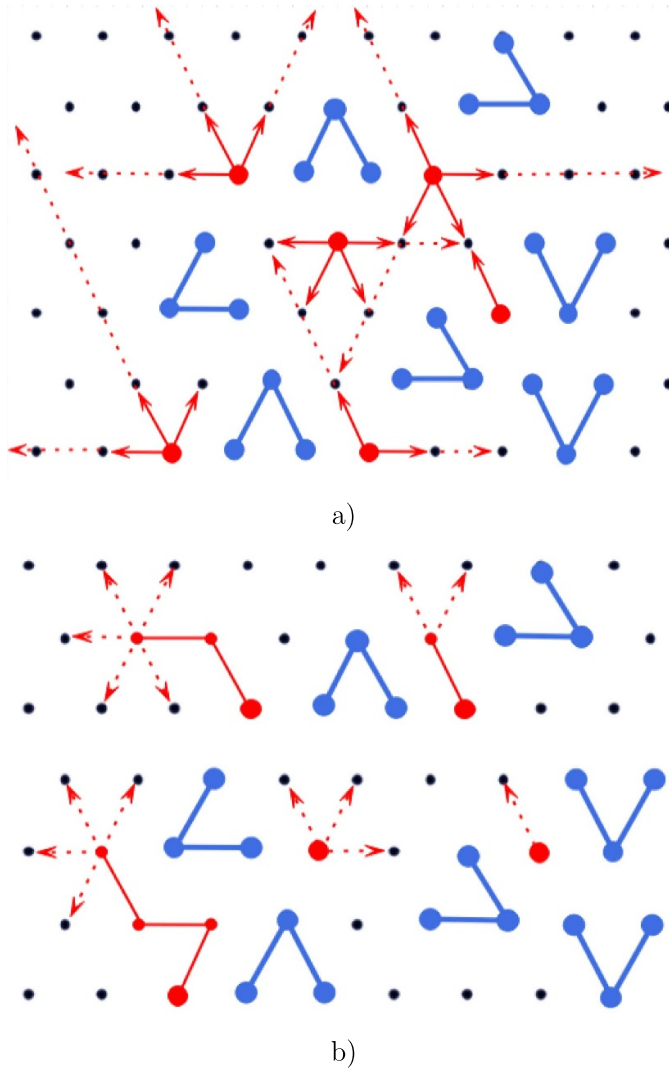
Figure 1. Illustration of the object growth for: (a) k-mers and (b) SARWs. The growing objects are red, and the triangle impurities are shown in blue. The red dashed lines show the possible growth directions.

without significant concern for finite-size effects [46–48] and the need for averaging over a large number of runs, as the system is self-averaging. Numerical studies have demonstrated that finite-size effects on a lattice of size L can be disregarded for object sizes $\leqslant L/8$ [20]. Therefore, Monte Carlo simulations are conducted on a triangular lattice up to a size of $L \leqslant 3200$.

3. Results and discussion

Percolation and jamming properties are studied for growing k-mers and growing SARWs on a triangular lattice. Simulations are performed for three different shapes of impurities covering three lattice sites—needle-like, angled, and triangular. Results are obtained for

a wide range of impurity concentrations ρ_{imp}, and for a wide range of initial monomer (seed) densities ρ.

3.1. Percolation

The values of the percolation thresholds for the infinitely large lattice θ_{p}^* are determined using the usual finite-size scaling analysis of percolation on 2D lattices [49]. In such systems, the effective percolation threshold θ_{p} approaches the asymptotic value θ_{p}^* for $L \to \infty$ via the power law:

$$\theta_{\text{p}} - \theta_{\text{p}}^* \propto L^{-1/\nu}. \tag{1}$$

Here, θ_{p}^* is the exact percolation threshold (as $L \to \infty$), and ν is the correlation length critical exponent. It should be noted that the universality class of random percolation in 2D is very well identified and the critical exponents are known, namely, $\nu \simeq 4/3$ [49, 50]. The latter relationship allows us to extrapolate the threshold for an infinite system, $L \to \infty$. This kind of behavior, which is expected for systems without long-range correlations, has been observed in previous studies of percolation of extended objects on 2D lattices [51–54].

Simulations were performed for lattice sizes ranging from $L = 100$ to $L = 3200$. Finite-size scaling of the percolation threshold θ_{p} for the growing k-mers (needle-like objects) and impurities of shape (D) is illustrated in figure 2(a), and for the growing SARWs and impurities of shape (B) in figure 2(b). Values of the percolation threshold θ_{p} vs $L^{-3/4}$ are shown for various seed densities ρ and for impurity concentrations $\rho_{\text{imp}} = 0.2$ and $\rho_{\text{imp}} = 0.25$ in the k-mers and SARWs, respectively. Plotting the obtained value θ_{p} of the percolation threshold for various lattice sizes against $L^{-1/\nu}$ confirms the validity of the finite-size scaling in the system and determines the asymptotic value of the percolation threshold θ_{p}^*.

According to the scaling theory, the standard deviation σ of the percolation threshold measured for a finite lattice L satisfies the power law:

$$\sigma \propto L^{-1/\nu}. \tag{2}$$

The standard deviation $\sigma(L)$ is calculated for the growing k-mers and for various seed densities ρ and initial impurity concentrations ρ_{imp}. In all the cases, we obtained confirmation of the power law of equation (2), with the value of the exponent $1/\nu$ ranging from 0.711 to 0.758. These results are in good agreement with the universal value $1/\nu = 3/4$ for 2D percolations. In figure 3, and all subsequent figures that show the values of the percolation thresholds, the error bars do not exceed the size of the symbols.

3.1.1. Impurities of shape (B). The results of the simulations of the object growth on a triangular lattice with needle-like impurities (k-mers covering three lattice sites) are shown in figures 3–5. Figure 3(a) shows the dependence of the percolation threshold θ_{p}^* on the seed density ρ and on the impurity concentration ρ_{imp} for the growing needle-like objects (k-mers). For a given impurity concentration, the percolation threshold increases with the seed density, reaches a maximum and slightly decreases for higher values of ρ in the lower impurity concentrations, but increases monotonically at the
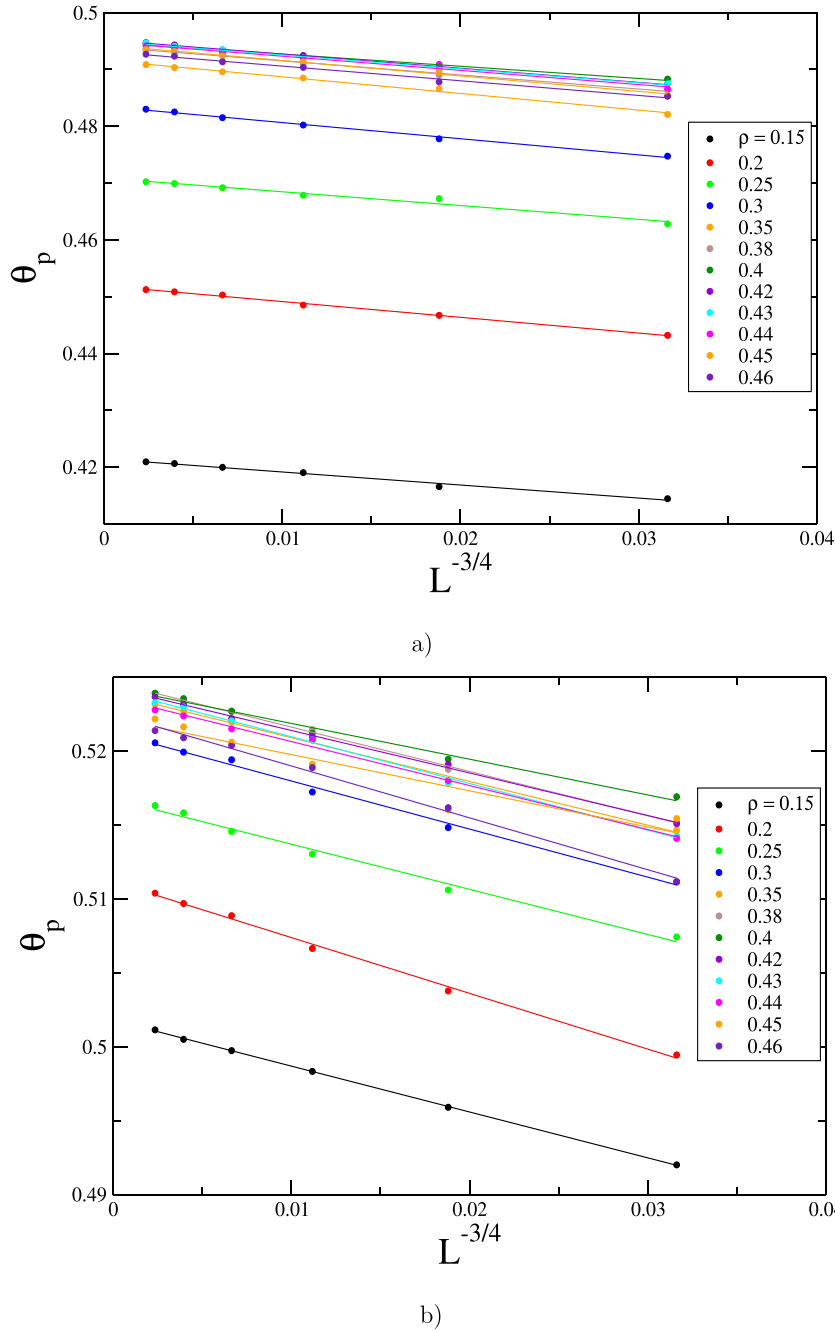
a)

b)

Figure 2. (a) Finite-size scaling of the percolation threshold θ_p against $L^{-1/\nu}$, with $\nu = 4/3$, for the growing needle-like objects (k-mers) and various values of the initial seed densities given in the legend. The impurities of shape (D) are distributed randomly at concentration $\rho_\mathrm{imp} = 0.2$; (b) finite-size scaling of the percolation threshold θ_p against $L^{-1/\nu}$, with $\nu = 4/3$, for the growing SARWs and various values of the initial seed densities given in the legend. The impurities of shape (B) are distributed randomly at concentration $\rho_\mathrm{imp} = 0.25$.
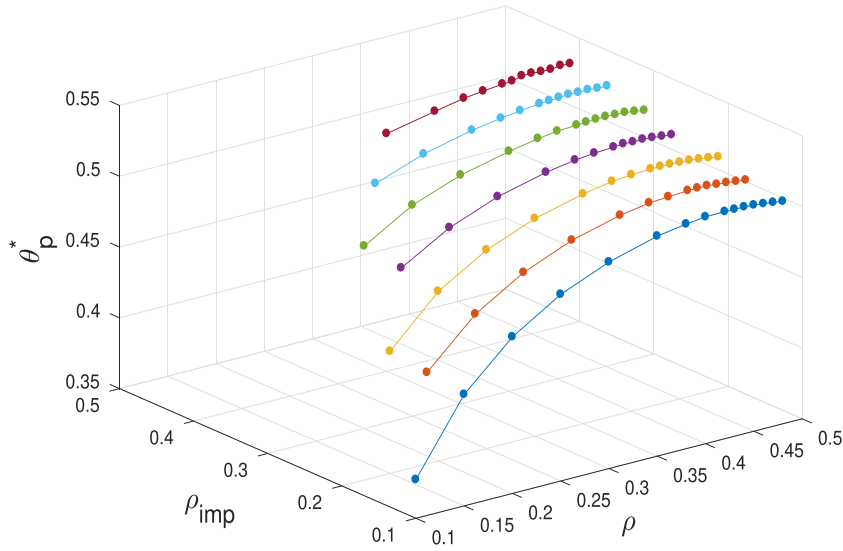
a)
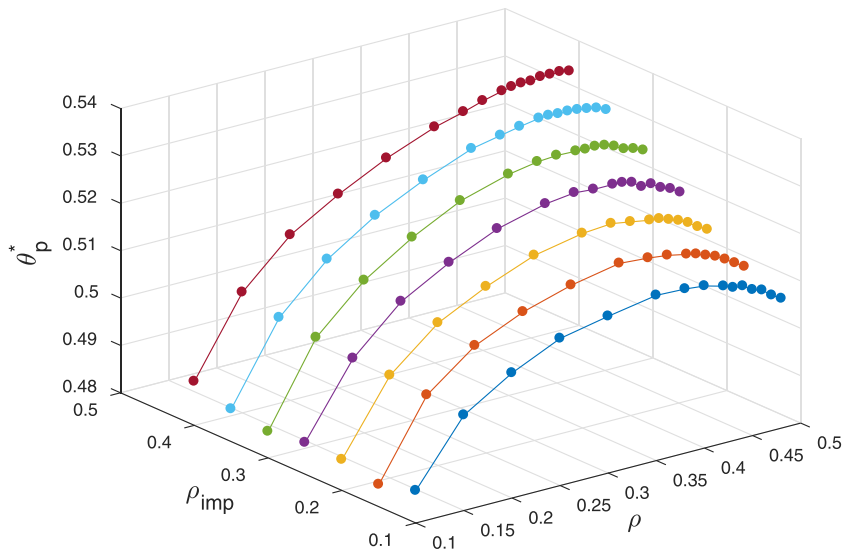
b)

Figure 3. (a) The dependence of the percolation threshold θ_{p}^{*} on the initial seed density ρ and on the impurity concentration ρ_{imp} for the growing k-mers in the presence of impurities of shape (B). (b) The dependence of the percolation threshold θ_{p}^{*} on the initial seed density ρ and on the impurity concentration ρ_{imp} for the growing SARWs in the presence of impurities of shape (B).

highest impurity concentrations. At low values of the seed densities, objects have enough space to grow, longer objects form a porous surface and the percolation threshold θ_{p}^{*} is reached at low values of the coverage. Higher seed density reduces the possibility of the object growth. As the seed density increases, the contribution of small objects to
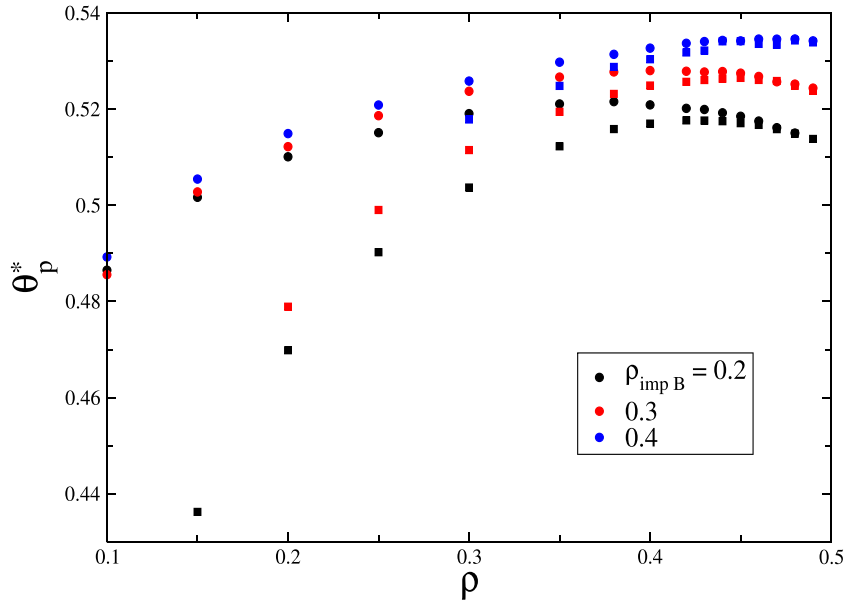
Figure 4. Comparison of the influence of the seed density ρ on the percolation threshold θ_p^* for the growing k-mers (squares) and for the growing SARW chains (circles). The dependence of θ_p^* on ρ is shown for three different values of the impurity concentration ρ_{imp} given in the legend. The impurities are shape (B).

the coverage increases and the percolation threshold is reached at higher coverages. At low values of the initial seed densities, the percolation threshold can only be reached for sufficiently low values of the impurity concentration. The initial seed density above which percolation can be reached increases with the growth of ρ_{imp}. The percolation threshold monotonically increases with the impurity concentration for all values of ρ. In the presence of impurities, it is more difficult to make connections between the growing objects, and the percolation cluster appears at higher coverages.

For the growth of the SARWs, the percolation threshold can be reached for all values of the impurity concentration investigated (figure 3(b)). These growing objects have a greater ability to avoid impurities and make connections. The percolation threshold increases with the seed density, reaches a maximum and decreases for higher values of ρ. The percolation threshold monotonically increases with the impurity concentration for all values of ρ. The structure of the coverings depends on the seed density ρ and on the impurity concentration ρ_{imp}. Basically, fractions of monomers, dimers and longer objects at the percolation threshold depend on the seed density ρ and on the impurity concentration ρ_{imp}. For lower values of ρ_{imp}, there is a value of ρ for which these fractions result in the highest values of the percolation thresholds [31].

Comparison of the influence of the seed density ρ on the percolation threshold θ_p^* for the growing k-mers (squares) and for the growing random walk chains (circles) is shown in figure 4. The dependence of θ_p^* on ρ is shown for three different values of the impurity concentration ρ_{imp}. It can be seen that the values of θ_p^* have lower values for the needle-like objects than for the SARW chains in the whole seed density range. This difference
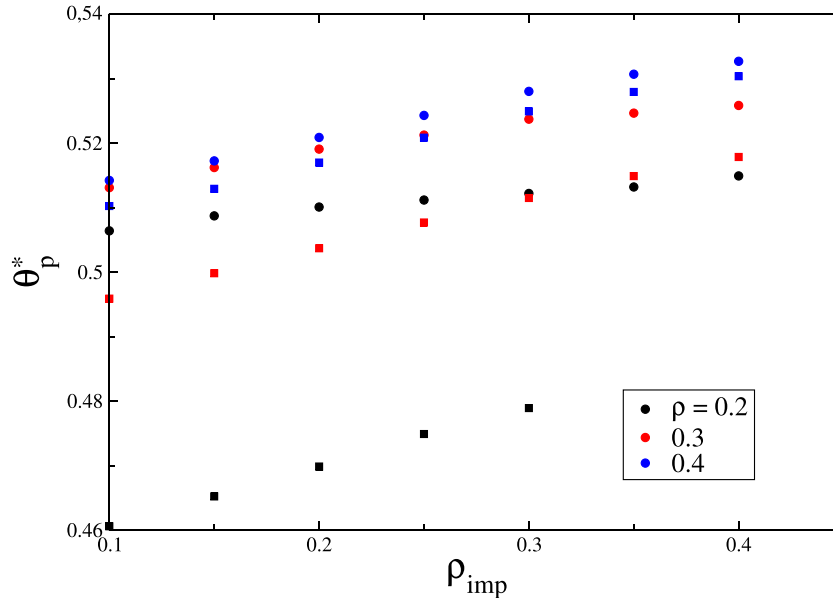
Figure 5. Comparison of the influence of the impurity concentration ρ_{imp} on the percolation threshold θ_p^* for the growing k-mers (squares) and for the growing SARW chains (circles). The dependence of θ_p^* on ρ_{imp} is shown for three different values of the seed densities ρ given in the legend. The impurities are shape (B).

is more prominent for lower values of the seed densities. Surface configurations that form during the growth of the needle-like objects are more porous than in the growth of the SARWs, and percolation occurs at lower coverage values for the needle-like objects. With the growth of the seed density ρ, this difference decreases and practically ceases when ρ approaches the value of the percolation threshold for monomers on the triangular lattice.

The influence of the impurity concentration ρ_{imp} on the percolation threshold θ_p^* for the growing k-mers and for the growing random walk chains is illustrated in figure 5. The dependence of θ_p^* on ρ_{imp} is shown for three different values of the seed densities ρ given in the legend. For given seed concentrations, the percolation thresholds have lower values for the k-mers than for the growing SARWs for all the impurity concentration values.

3.1.2. Impurities of shape (C). The dependence of the percolation threshold θ_p^* for the growing needle-like objects (k-mers) on the seed density ρ and on the impurity concentration ρ_{imp} is shown in figure 6(a). Similarly, the dependence of θ_p^* on the seed density and on the impurity concentration for the growing SARWs is illustrated in figure 6(b).

For the angled impurity shape, the percolation threshold increases monotonically with the seed density for the highest values of the impurity concentrations. For lower impurity concentrations, the percolation threshold increases with the seed density, reaches a maximum and slightly decreases for higher values of ρ. Except for the lowest seed concentrations considered for the growth of the SARWs, the percolation threshold
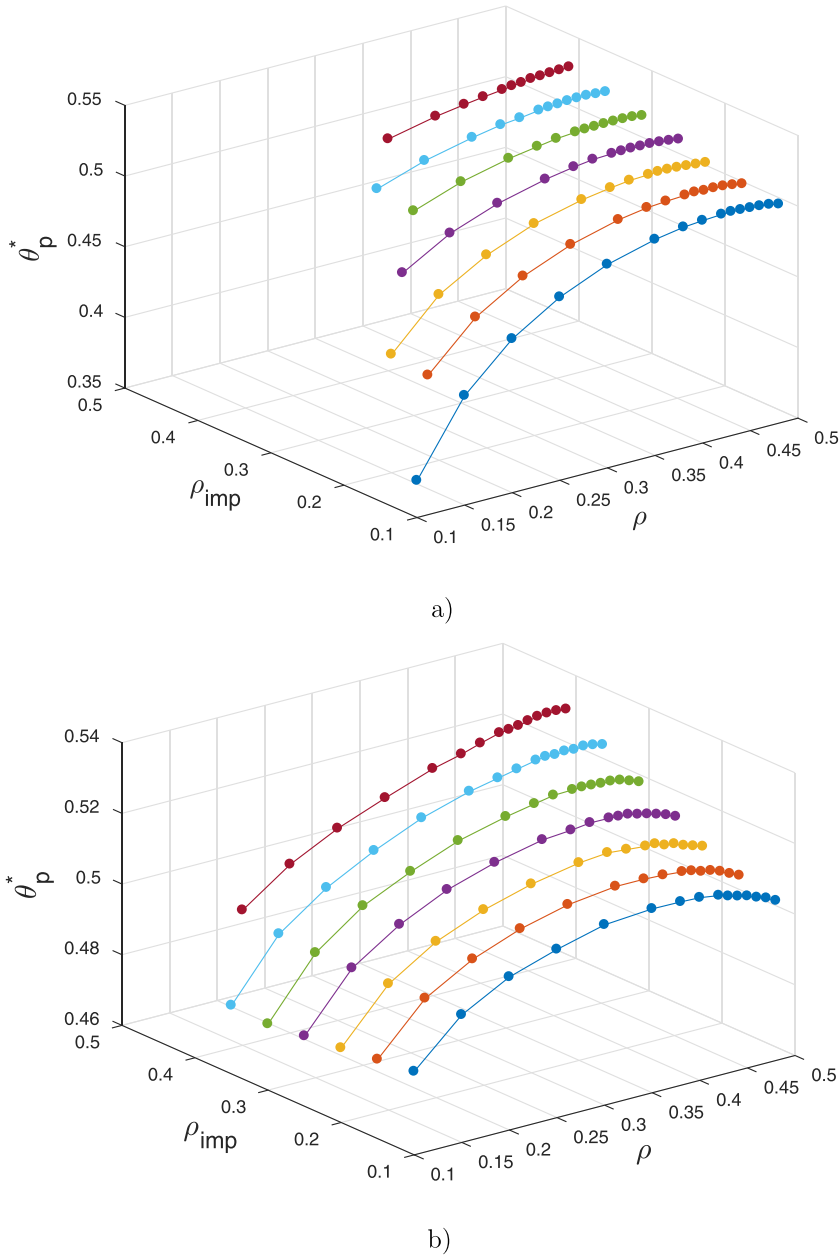
a)

b)

Figure 6. (a) The dependence of the percolation threshold θ_{p}^* on the initial seed density ρ and on the impurity concentration ρ_{imp} for the growing k-mers in the presence of impurities of shape (C). (b) The dependence of the percolation threshold θ_{p}^* on the initial seed density ρ and on the impurity concentration ρ_{imp} for the growing SARWs in the presence of impurities of shape (C).

increases with the impurity concentration ρ_{imp}. It can be seen that the presence of angled impurities has a qualitatively similar influence on the percolation threshold to the presence of the needle-like impurities of shape (B).
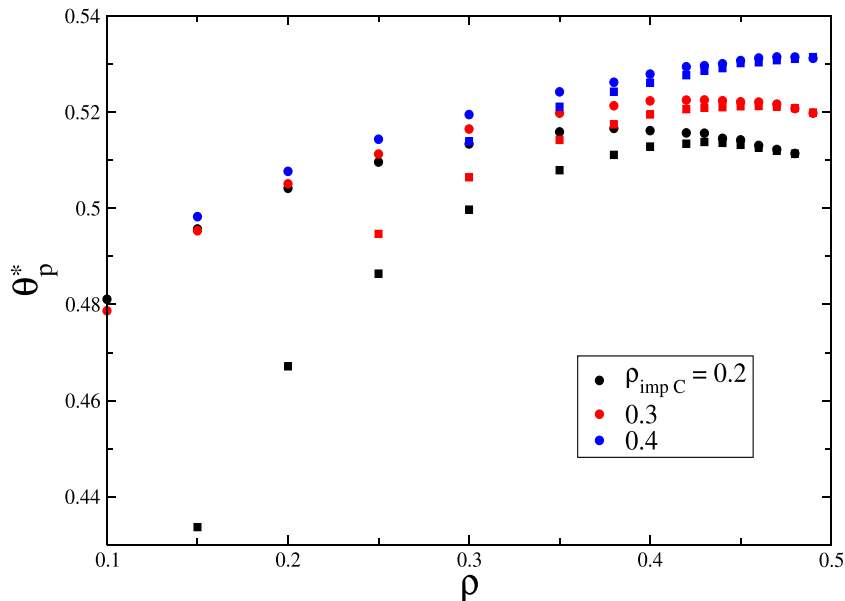
Figure 7. Comparison of the influence of the seed density ρ on the percolation threshold θ_{p}^{*} for the growing k-mers (squares) and for the growing SARW chains (circles). The dependence of θ_{p}^{*} on ρ is shown for three different values of the impurity concentration ρ_{imp} given in the legend. The impurities are shape (C).

Figure 7 gives a comparison of the influence of the seed density ρ on the percolation threshold θ_{p}^{*} for the growing k-mers and for the growing SARW chains. At a given impurity concentration, the growing SARWs have higher percolation thresholds than the growing needle-like objects (k-mers). A comparison of the influence of the impurity concentration ρ_{imp} on the percolation threshold θ_{p}^{*} for the growing k-mers and for the growing random walk chains is given in figure 8. At a given seed concentration, the growing SARWs have higher percolation thresholds than the growing needle-like objects.

3.1.3. Impurities of shape (D). The dependence of the percolation threshold θ_{p}^{*} on the seed density ρ and on the impurity concentration ρ_{imp} for the triangular lattice covered with impurities of a triangular shape is shown in figure 9. Figure 9(a) illustrates the dependence of the percolation threshold on ρ and ρ_{imp} for the k-mer growth. It can be seen that for the growing k-mers, θ_{p}^{*} increases with the seed density, reaches a maximum and decreases for higher values of ρ. The percolation threshold increases monotonically with the seed density for only the highest value of the impurity concentration considered. On the other hand, θ_{p}^{*} slightly decreases with the impurity concentration for given values of the seed concentration.

When the growing objects are the SARWs, the dependence of the percolation threshold on the seed density is qualitatively similar, but with larger differences in θ_{p}^{*} for various impurity concentrations ρ_{imp} (figure 9(b)). In the SARWs growth, θ_{p}^{*} decreases more abruptly with the triangular impurity concentration than in the needle-like-objects. SARWs can avoid the impurities more easily than the needle-like objects,
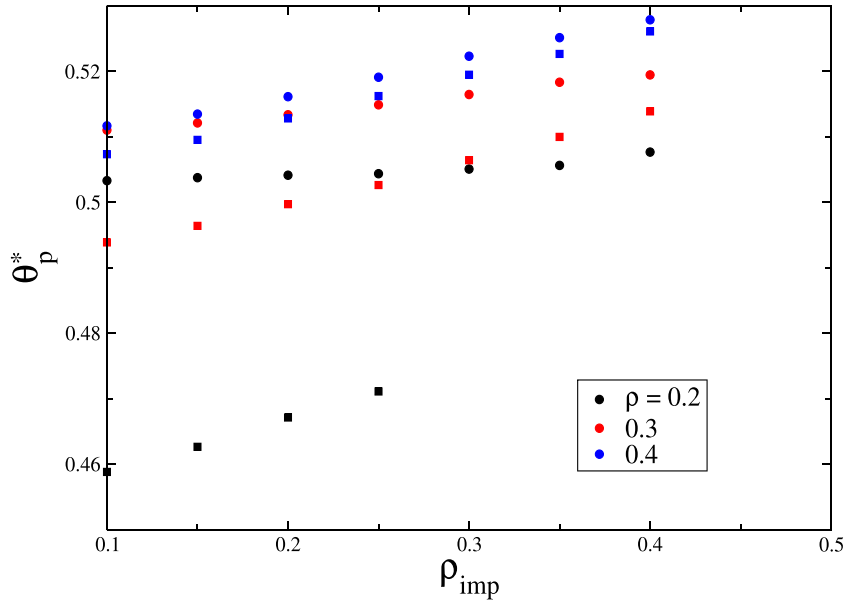
Figure 8. Comparison of the influence of the impurity concentration ρ_{imp} on the percolation threshold θ_p^* for the growing k-mers (squares) and for the growing SARW chains (circles). The dependence of θ_p^* on ρ_{imp} is shown for three different values of the seed densities ρ given in the legend. The impurities are shape (C).

and the impurities of a triangular shape are more easily avoided. It seems that the existence of the impurities of a triangular shape facilitates percolation.

A comparison of the percolation properties in the needle-like objects growth to the SARWs growth in the presence of impurities of a triangular shape is shown in figures 10 and 11. The dependence of the percolation threshold θ_p^* on the seed density ρ for three different values of the impurity concentrations is shown in figure 10, and the dependence of the percolation threshold θ_p^* on the impurity concentration ρ_{imp} for three different seed concentrations is shown in figure 11. Both figures clearly indicate that percolation is reached at lower coverages in the growing needle-like objects.

3.1.4. The influence of impurity shape—comparisons. Figures 12 and 13 illustrate the impact of the impurity shape on the percolation properties of the growing k-mers and of the growing SARWs. The dependence of the percolation threshold on the seed density is shown for the triangular lattice with needle-like, angled and triangular impurities. The results for the triangular lattice with point-like impurities, given in detail elsewhere [31], are also shown for the sake of comparison. The dependence of θ_p^* on the seed density is shown in figure 12(a) for the growing k-mers, and in figure 12(b) for the growing SARWs. For a fixed impurity concentration, the largest percolation thresholds are obtained for the needle-like impurities (B), slightly lower values of θ_p^* are obtained in the presence of angled impurities (C) and the lowest percolation thresholds are found for the impurities with a triangular shape (D).

The dependence of θ_p^* on the impurity concentration is shown in figures 13(a) and (b) for the growing k-mers and for the growing SARWs, respectively. In the presence of
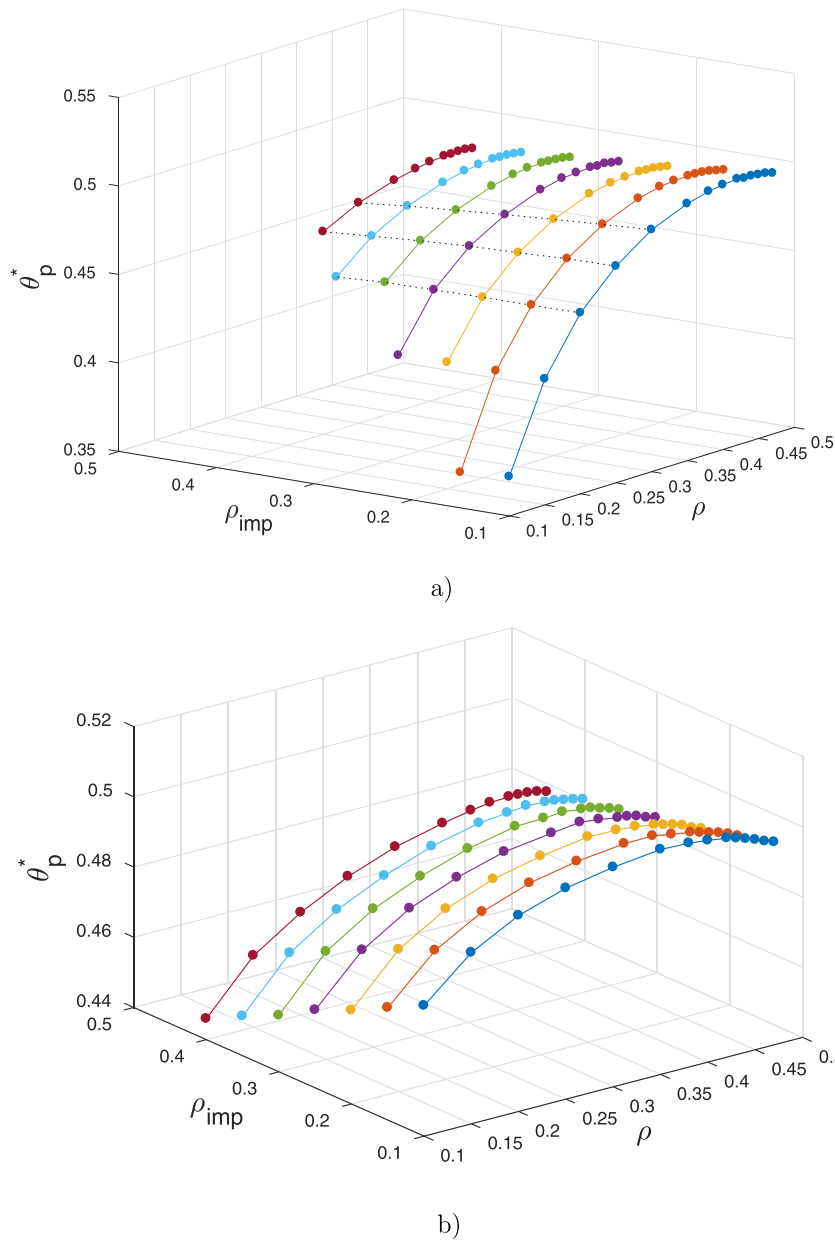
a)

b)

Figure 9. (a) The dependence of the percolation threshold θ_{p}^{*} on the initial seed density ρ and on the impurity concentration ρ_{imp} for the growing k-mers in the presence of impurities of shape (D). The dotted lines are only for the visualization. (b) The dependence of the percolation threshold θ_{p}^{*} on the initial seed density ρ and on the impurity concentration ρ_{imp} for the growing SARWs in the presence of impurities of shape (D).

needle-like and angled impurities, the percolation threshold increases with the impurity concentration for a fixed seed density. The percolation thresholds have the highest values in the needle-like impurities, and somewhat lower values in the angled impurities. For the growing objects, avoidance is most difficult for the needle-like shaped impurities. On
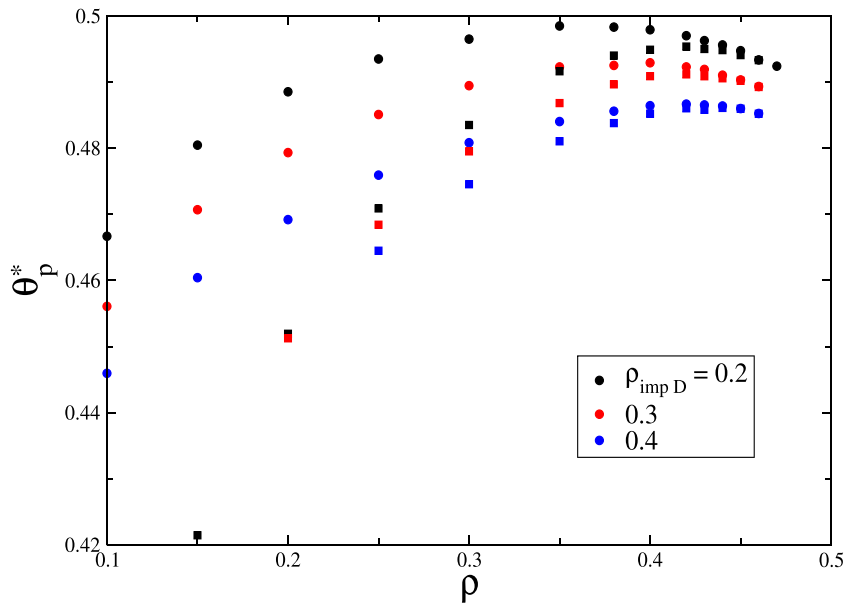
Figure 10. Comparison of the influence of the seed density ρ on the percolation threshold θ_p^* for the growing k-mers (squares) and for the growing SARW chains (circles). The dependence of θ_p^* on ρ is shown for three different values of the impurity concentration ρ_{imp} given in the legend. The impurities are shape (D).
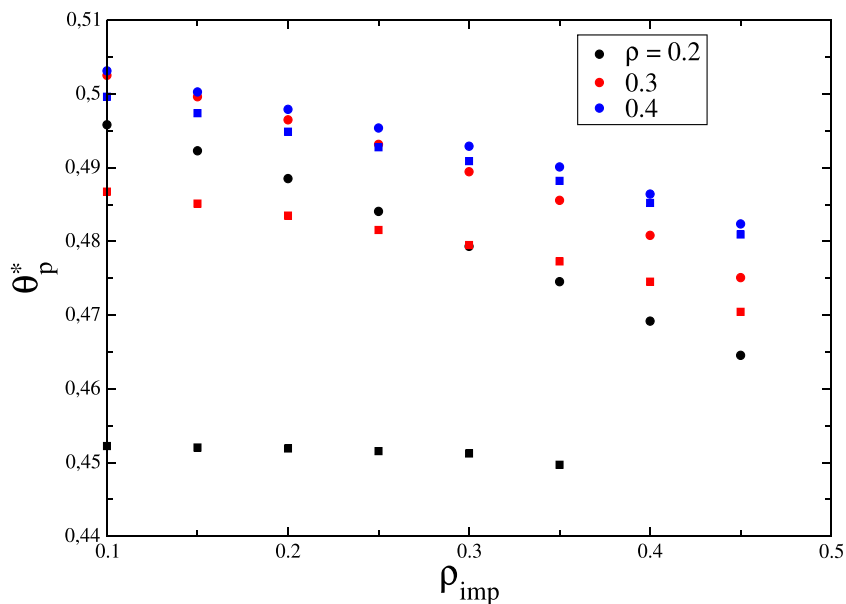

Figure 11. Comparison of the influence of the impurity concentration ρ_{imp} on the percolation threshold θ_p^* for the growing k-mers (squares) and for the growing SARW chains (circles). The dependence of θ_p^* on ρ_{imp} is shown for three different values of the seed densities ρ given in the legend. The impurities are shape (D).

a)

b)
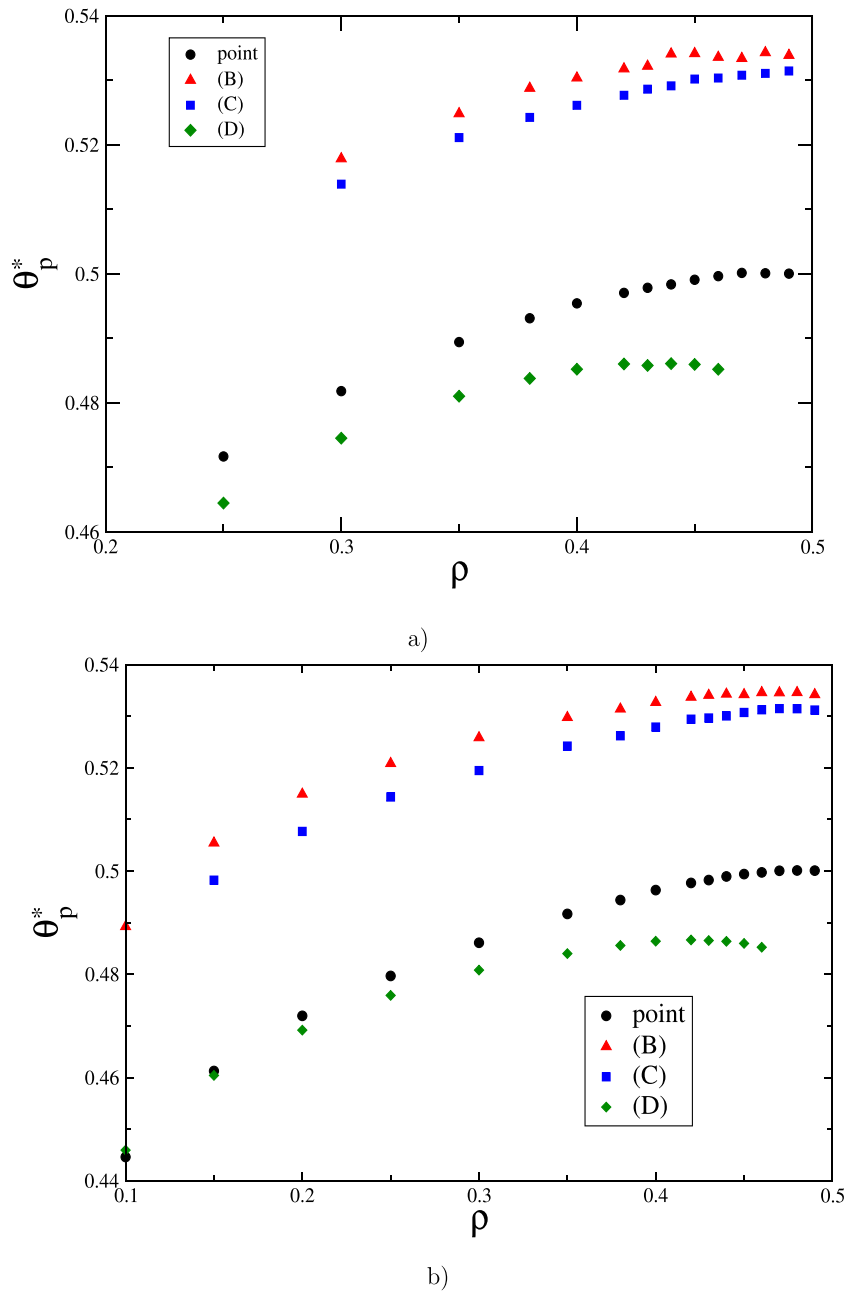
Figure 12. (a) Values of the percolation threshold θ_{p}^{*} as a function of the seed density ρ in the growth of k-mers. The fraction of the sites covered by the impurities is $\rho_{\mathrm{imp}} = 0.4$, and the types of impurities are indicated in the legend. (b) Values of the percolation threshold θ_{p}^{*} as a function of the seed density ρ in the growth of SARWs. The fraction of the sites covered by the impurities is $\rho_{\mathrm{imp}} = 0.4$, and the types of impurities are indicated in the legend.

the other hand, in the presence of the triangular impurities, the percolation threshold decreases with the concentration of impurities. Triangular obstacles, being compact, can easily be avoided by the growing objects. Moreover, for larger concentrations of
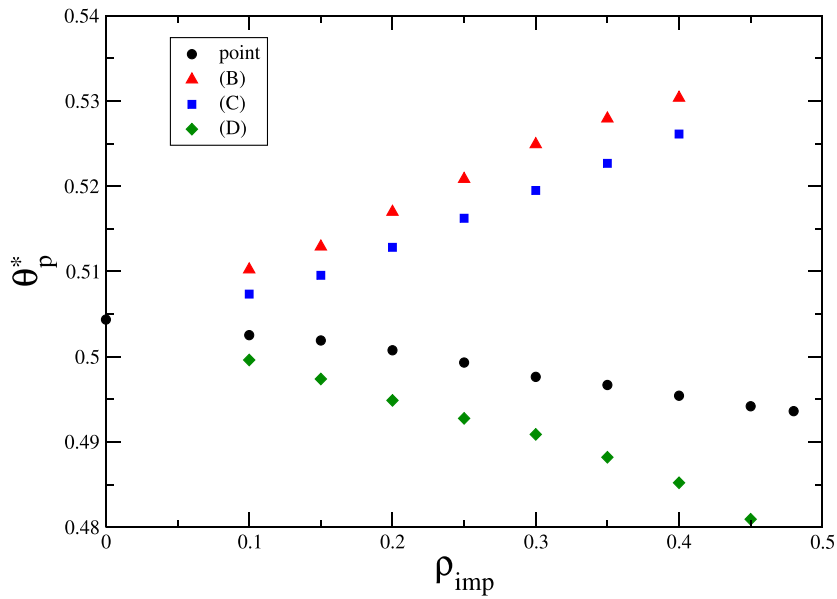
a)
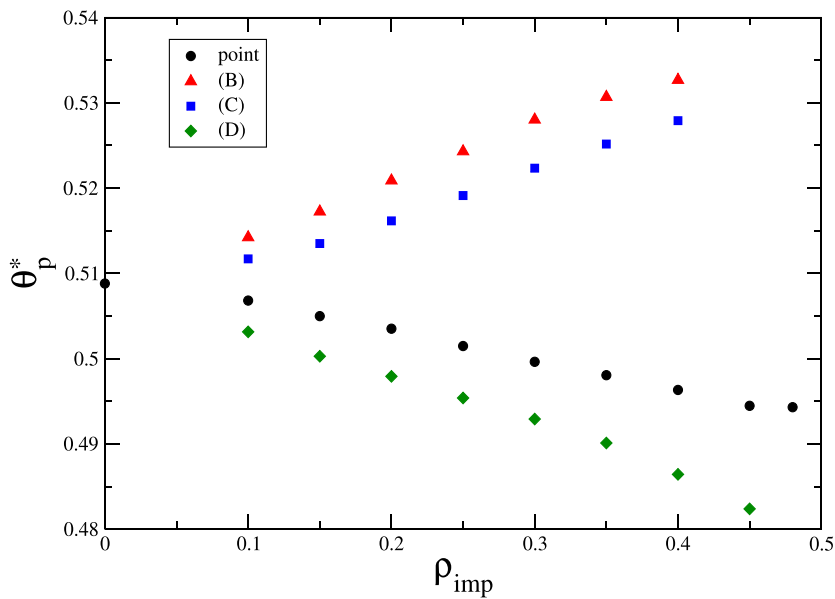
b)

Figure 13. (a) Values of the percolation threshold θ_{p}^* as a function of the impurity concentration ρ_{imp} in the growth of k-mers. The seed density is $\rho = 0.4$, and the types of impurities are indicated in the legend. (b) Values of the percolation threshold θ_{p}^* as a function of the impurity concentration ρ_{imp} in the growth of SARWs. The seed density is $\rho = 0.4$, and the types of impurities are indicated in the legend.
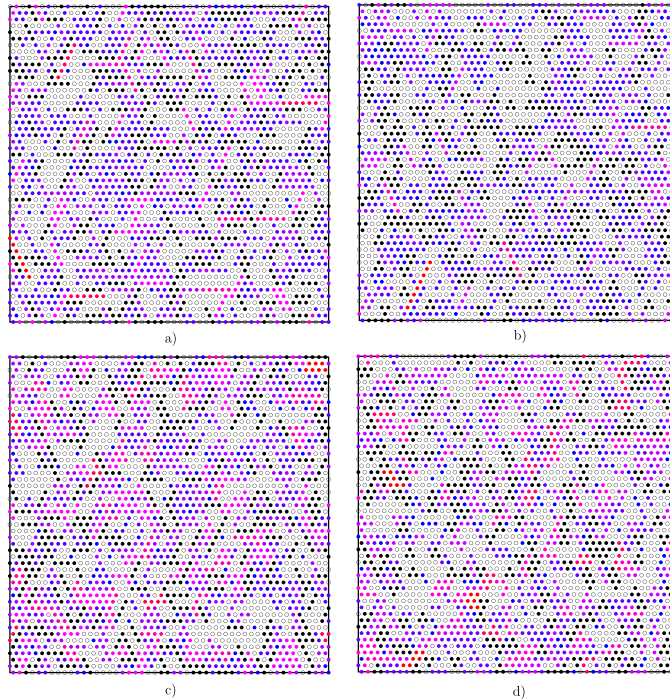
Figure 14. Typical configurations for the growth of: (a) k-mers on the lattice with impurities of type (B); (b) k-mers on the lattice with impurities of type (D); (c) SARWs on the lattice with impurities of type (B); (d) SARWs on the lattice with impurities of type (D). The snapshots are made at the moment of percolation cluster formation. Objects of different sizes are distinguished by color. The monomers are shown in blue and the longest objects in red. Impurities are black, while the empty lattice nodes are shown as open circles.

these impurities, growing objects have limited paths for growth and the surface is more porous, causing lower percolation threshold values.

Snapshots of the surface configurations at the percolation threshold are shown in figure 14 for k-mers and SARWs for two types of impurities: (B) and (D). Objects of different sizes are distinguished by color. The monomers are shown in blue and the longest objects in red. Different shades of purple correspond to different object lengths between these two. From comparison of figures 14(a) and (b) it can be seen that in the presence of the triangular impurities (D), a small fraction of growing needle-like objects can reach longer lengths than in the presence of the needle-like impurities (B). The length distribution of the objects differs in these two cases and leads to lower percolation threshold values in the triangular impurities. The growing SARWs can avoid the impurities more easily than the needle-like objects, resulting in larger fractions of longer objects in the surface configurations (figures 14(c) and (d)).

3.2. Jamming

The values of the jamming coverage θ_J for the growing needle-like objects are shown in figure 15 as a function of the initial seed density ρ and the impurity concentration ρ_{imp},
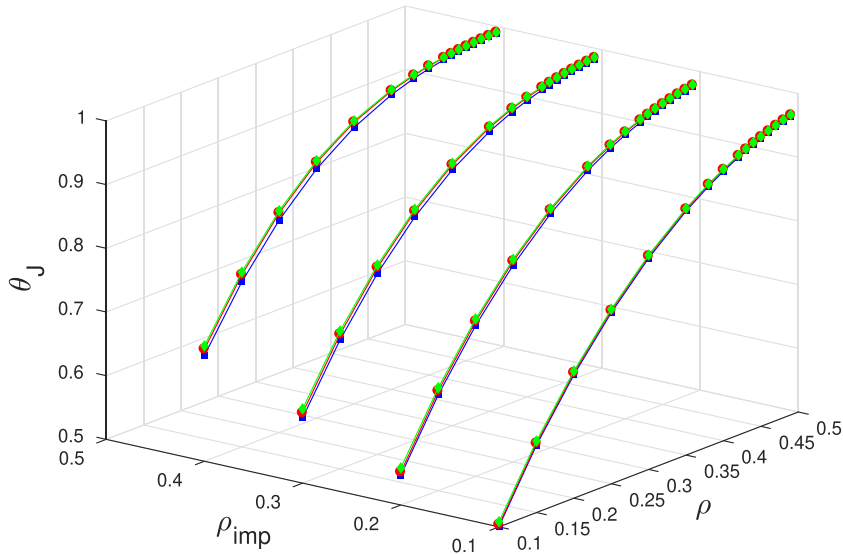
Figure 15. Values of the jamming coverage θ_J as a function of the impurity concentration ρ_{imp} and on the initial seed density ρ for the growing k-mers in the presence of impurities of shapes (B) (red circles), (C) (blue squares) and (D) (green diamonds).

Figure 16. Values of the jamming coverage θ_J as a function of the impurity concentration ρ_{imp} and on the initial seed density ρ for the growing SARWs in the presence of impurities of shapes (B) (red circles), (C) (blue squares) and (D) (green diamonds).
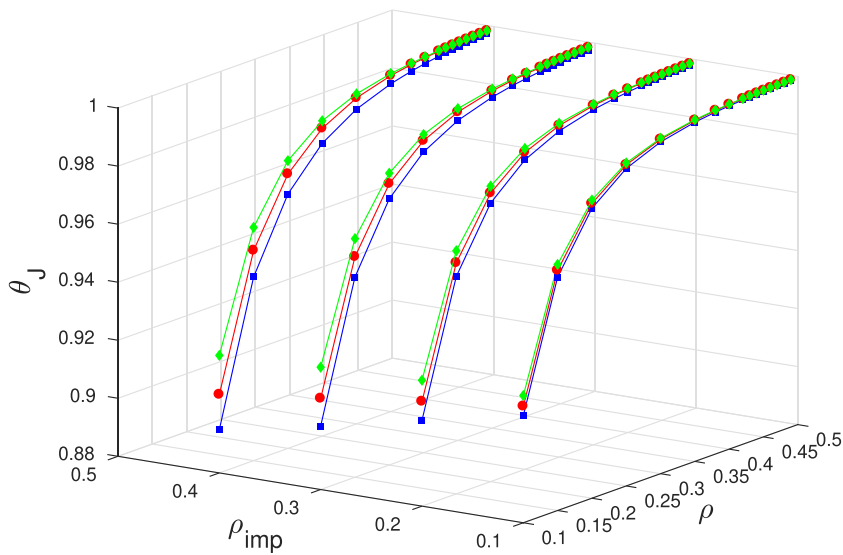
for various impurity shapes—needle-like, angled and triangular. The same dependence is shown in figure 16 for the growing SARWs. As expected, larger seed density provides growth of more objects, especially including the short ones, covering the surface more efficiently.

For a given ρ, θ_J decreases with ρ_{imp}, since larger impurity concentrations leave less space for the object's growth. Unlike the percolation threshold θ_{p}^*, the jamming coverage is only slightly affected by the shape of impurities. This impact is a little more pronounced in the growing SARWs. Jamming coverages have the highest values in the substrates with impurities of a triangular shape, and the lowest values in the angled impurities. Triangular impurities are most easily avoided by the growing objects, while the presence of angled impurities causes an increase in the number of blocked sites. In figures 15 and 16, the error bars do not exceed the size of the symbols.

4. Concluding remarks

Percolation and jamming properties were studied in a seeded growth model on a triangular lattice with finite-size impurities. Impurities of various shapes—needle-like, angled or triangular—were distributed on the lattice at random. The growing objects were the needle-like shapes and the random walk chains. Simulations were performed for various seed concentrations ρ up to the percolation threshold for monomer deposition, and also for various impurity concentrations ρ_{imp}.

For fixed seed densities and impurity concentrations, the percolation thresholds always have lower values in the k-mer growth than in the growth of the SARW chains. The growing needle-like objects form more porous surfaces, and the percolation is reached at lower values of the coverage fraction. On the other hand, the growing SARWs cover the surface more efficiently, resulting in higher percolation threshold values.

Our results suggest that the percolation properties in the seeded growth model are not only affected by the seed concentration and the impurity concentration, but also by the shape of impurities. For a given seed density, the percolation threshold increases with the impurity concentration in the needle-like and angled shaped impurities, but decreases in the point-like and triangular impurities. Percolation is most easily reached at high concentrations of triangular impurities. On the other hand, it is most difficult to achieve percolation at high concentrations of needle-like impurities. It seems that the placement of obstacles on the substrate can facilitate percolation or make it more difficult, depending on the obstacle shape.

As far as the jamming coverage is concerned, only a slight dependence on the shape of impurities is observed. This impact is a little more pronounced in the growing SARWs. Jamming coverages have the highest values in the substrates with triangular-shaped impurities, and the lowest values in the angled impurities. The triangular impurities are more easily avoided by the growing SARWs, causing the highest jamming coverages.

Acknowledgments

the PARADOX supercomputing facility at the Scientific Computing Laboratory of the Institute of Physics Belgrade.

References

[1] Goodman D W 2008 Precious little catalyst *Nature* **454** 948–9
[2] Peng S, Lee Y, Wang C, Yin H, Dai S and Sun S 2008 A facile synthesis of monodisperse Au nanoparticles and their catalysis of CO oxidation *Nano Res.* **1** 229–34
[3] Hashmi A S K 2007 Raising the gold standard *Nature* **449** 292–3
[4] Lee C *et al* 2002 Molecular wires and gold nanoparticles as molewares for the molecular scale electronics *Curr. Appl. Phys.* **2** 39–45
[5] Morandi V, Marabelli F, Amendola V, Meneghetti M and Comoretto D 2007 Colloidal photonic crystals doped with gold nanoparticles: spectroscopy and optical switching properties *Adv. Funct. Mater.* **17** 2779–86
[6] Pileni M-P 2001 Magnetic fluids: fabrication, magnetic properties and organization of nanocrystals *Adv. Funct. Mater.* **11** 323–36
[7] He W, Henne W A, Wei Q, Zhao Y, Doorneweerd D D, Cheng J-X, Low P S and Wei A 2008 Two-photon luminescence imaging of bacillus spores using peptide-functionalized gold nanorods *Nano Res.* **1** 450–6
[8] Tansil N C and Gao Z 2006 Nanoparticles in biomolecular detection *Nano Today* **1** 28–37
[9] Chithrani B D, Ghazani A A and Chan W C W 2006 Determining the size and shape dependence of gold nanoparticle uptake into mammalian cells *Nano Lett.* **6** 662–8
[10] Anshup A, Sai Venkataraman J, Subramaniam C, Rajeev Kumar R, Priya S, Santhosh Kumar T R, Omkumar R V, John A and Pradeep T 2005 Growth of gold nanoparticles in human cells *Langmuir* **21** 11562–7
[11] Koga K, Ikeshoji T and Sugawara K 2004 Size- and temperature-dependent structural transitions in gold nanoparticles *Phys. Rev. Lett.* **92** 115507
[12] Park J Y, Jung I O, Moon J H, Lee B-T and Kim S S 2005 Temperature induced shape change of highly aligned ZnO nanocolumns *J. Cryst. Growth* **282** 353–8
[13] Manna L, Scher E C and Paul Alivisatos A 2002 Shape control of colloidal semiconductor nanocrystals *J. Cluster Sci.* **13** 521–32
[14] Nikoobakht B and El-Sayed M A 2003 Preparation and growth mechanism of gold nanorods (nrs) using seed-mediated growth method *Chem. Mater.* **15** 1957–62
[15] Gole A and Murphy C J 2004 Seed-mediated synthesis of gold nanorods: role of the size and nature of the seed *Chem. Mater.* **16** 3633–40
[16] Habas S E, Lee H, Radmilovic V, Somorjai G A and Yang P 2007 Shaping binary metal nanocrystals through epitaxial seeded growth *Nat. Mater.* **6** 692–7
[17] Lohse S E and Murphy C J 2013 The quest for shape control: a history of gold nanorod synthesis *Chem. Mater.* **25** 1250–61
[18] Roy B and Santra. S B 2017 First-order transition in a percolation model with nucleation and preferential growth *Phys. Rev.* E **95** 010101
[19] Evans J W 1993 Random and cooperative sequential adsorption *Rev. Mod. Phys.* **65** 1281–329
[20] Manna S S and Švrakić N M 1991 Random sequential adsorption: line segments on the square lattice *J. Phys. A: Math. Gen.* **24** L671–6
[21] Talbot J, Tarjus G, Van Tassel P R and Viot P 2000 From car parking to protein adsorption: an overview of sequential adsorption processes *Colloids Surf.* A **165** 287–324
[22] Budinski-Petković L, Lončarević I, Dujak D, Karač A, Šćepanović J R, Jakšić Z M and Vrhovac S B 2017 Particle morphology effects in random sequential adsorption *Phys. Rev.* E **95** 022114
[23] Kondrat G 2008 Impact of composition of extended objects on percolation on a lattice *Phys. Rev.* E **78** 011101
[24] Ziff R M 2009 Explosive growth in biased dynamic percolation on two-dimensional regular lattice networks *Phys. Rev. Lett.* **103** 045701
[25] Tsakiris N, Maragakis M, Kosmidis K and Argyrakis P 2010 Percolation of randomly distributed growing clusters: finite-size scaling and critical exponents for the square lattice *Phys. Rev.* E **82** 041108
[26] Ioselevich A S and Kornyshev A A 2002 Approximate symmetry laws for percolation in complex systems: percolation in polydisperse composites *Phys. Rev.* E **65** 021301
[27] Tarasevich Y Y, Lebovka N I and Laptev V V 2012 Percolation of linear k-mers on a square lattice: from isotropic through partially ordered to completely aligned states *Phys. Rev.* E **86** 061116

[28] Budinski-Petković L, Lončarević I, Petković M, Jakšić Z M and Vrhovac S B 2012 Percolation in random sequential adsorption of extended objects on a triangular lattice *Phys. Rev.* E **85** 061117

[29] Cohen R, Erez K, ben Avraham D and Havlin S 2001 Breakdown of the internet under intentional attack *Phys. Rev. Lett.* **86** 3682–5

[30] Dujak D, Karač A, Budinski-Petković L, Jakšić Z M and Vrhovac S B 2022 Percolation and jamming properties in particle shape-controlled seeded growth model *Eur. Phys. J.* B **95** 143

[31] Dujak D, Karač A, Budinski-Petković L, Jakšić Z M and Vrhovac S B 2023 Percolation and jamming properties in object growth model on a lattice with impurities *J. Stat. Mech.* 023204

[32] Roy B and Santra S B 2018 Finite size scaling study of a two parameter percolation model: constant and correlated growth *Physica* A **492** 969–79

[33] Carrey J and Maurice J-L 2001 Transition from droplet growth to percolation: Monte Carlo simulations and an analytical model *Phys. Rev.* B **63** 245408

[34] Adamson A W and Gast A P 1997 *Physical Chemistry of Surfaces* 6th edn (Wiley)

[35] Cadilhe A, Araújo N A M and Privman V 2007 Random sequential adsorption: from continuum to lattice and pre-patterned substrates *J. Phys.: Condens. Matter* **19** 065124

[36] Cornette V, Ramirez-Pastor A J and Nieto F 2006 Percolation of polyatomic species on site diluted lattices *Phys. Lett.* A **353** 452–8

[37] Cornette V, Ramirez-Pastor A J and Nieto F 2006 Percolation of polyatomic species with the presence of impurities *J. Chem. Phys.* **125** 204702

[38] Centres P M and Ramirez-Pastor A J 2015 Percolation and jamming in random sequential adsorption of linear k-mers on square lattices with the presence of impurities *J. Stat. Mech.* P10011

[39] Tarasevich Y Y, Laptev V V, Vygornitskii N V and Lebovka N I 2015 Impact of defects on percolation in random sequential adsorption of linear k-mers on square lattices *Phys. Rev.* E **91** 012109

[40] Tarasevich Y Y, Laptev V V, Goltseva V A and Lebovka N I 2017 Influence of defects on the effective electrical conductivity of a monolayer produced by random sequential adsorption of linear k-mers onto a square lattice *Physica* A **477** 195–203

[41] Lončarević I, Budinski-Petković L, Dujak D, Karač A, Jakšić Z M and Vrhovac S B 2017 The study of percolation with the presence of extended impurities *J. Stat. Mech.* 093202

[42] Cornette V, Ramirez-Pastor A J and Nieto F 2011 Random sequential adsorption of polyatomic species with the presence of impurities *Physica* A **390** 671–9

[43] Ziff R M and Newman M E J 2002 Convergence of threshold estimates for two-dimensional percolation *Phys. Rev.* E **66** 016129

[44] Swendsen R H 1981 Dynamics of random sequential adsorption *Phys. Rev.* A **24** 504–8

[45] Hinrichsen E L, Feder J and Jssang T 1986 Geometry of random sequential adsorption *J. Stat. Phys.* **44** 793–827

[46] Evans J W, Burgess D R and Hoffman D K 1984 Irreversible random and cooperative processes on lattices: spatial correlations *J. Math. Phys.* **25** 3051–63

[47] Bonnier B, Hontebeyrie M, Leroyer Y, Meyers C and Pommiers E 1994 Adsorption of line segments on a square lattice *Phys. Rev.* E **49** 305–12

[48] Lebovka N I, Karmazina N N, Tarasevich Y Y and Laptev V V 2011 Random sequential adsorption of partially oriented linear k-mers on a square lattice *Phys. Rev.* E **84** 061603

[49] Aharony A and Stauffer D 2003 *Introduction to Percolation Theory* revised 2nd edn (Taylor and Francis)

[50] Sykes M F, Glen M and Gaunt D S 1974 The percolation probability for the site problem on the triangular lattice *J. Phys. A: Math. Nucl. Gen.* **7** L105

[51] Ramirez-Pastor A J, Centres P M, Vogel E E and Valdés J F 2019 Jamming and percolation for deposition of k^2-mers on square lattices: a Monte Carlo simulation study *Phys. Rev.* E **99** 042131

[52] Perino E J, Matoz-Fernandez D A, Pasinetti P M and Ramirez-Pastor A J 2017 Jamming and percolation in random sequential adsorption of straight rigid rods on a two-dimensional triangular lattice *J. Stat. Mech.* 073206

[53] Lebrecht W, Vogel E E, Valdés J F, Ramirez-Pastor A J, Centres P M, González M I and Nieto F D 2015 Site trimer percolation on square lattices *Phys. Rev.* E **92** 012129

[54] Melchert O 2013 Universality class of the two-dimensional randomly distributed growing-cluster percolation model *Phys. Rev.* E **87** 022115